

Assessing Disability Glare Potential Due to Reflections from New Constructions: A Case Study Analysis and Recommendations for the Future

J. Alstan Jakubiec(*,♦) and Christoph F. Reinhart(**)

* E-Mail: alstan@jakubiec.net
Department of Architecture, Massachusetts Institute of Technology
77 Massachusetts Ave, Rm 5-418
Cambridge, MA 02139, USA
Telephone: (912) 247-1086, Fax: (617) 253-6152

** E-Mail: creinhart@mit.edu
Department of Architecture, Massachusetts Institute of Technology
77 Massachusetts Ave, Rm 5-418
Cambridge, MA 02139, USA
Telephone: (617) 253-7714, Fax: (617) 253-6152

♦ Corresponding Author

ABSTRACT

Disability glare, visual impairment due to extreme brightness or contrast, can be caused by intense reflections from new constructions nearby existing transportation or building infrastructure. A case study analysis is performed of a disability glare hazard at an airport created by the installation of a large array of photovoltaic panels between an air traffic control tower and the aircraft taxiway. The panels reflect blinding quantities of daylight into the control tower, produce temporary after images and dangerously obscure taxiing aircraft. The existing FAA guidelines for installation of solar technologies are discussed relative their shortcomings in identifying the glare hazard.

High dynamic range photography is used to analyze the glaring situation at the airport, and the authors propose a maximum brightness threshold of $30,000 \text{ cd/m}^2$ based on the physiology of human vision and the brightness of tasks necessary for air traffic controllers at the case-study airport. Detailed reflectivity and three-dimensional models of the photovoltaic panels and the airport are created and validated against measured data. Using these models, an annual analysis is performed of the glare hazard. This analysis is displayed temporally using graphs and spatially using images that indicate where the glaring reflections originate. Such information is useful in identifying the potential for disability glare before new constructions are built. Finally, the authors use the new method to analyze designs for remediation of the glare hazard.

INTRODUCTION

New constructions such as photovoltaic (PV) panels or buildings can cause glare due to intense reflections of sunlight from their surfaces. Such reflections can literally occur in blinding quantities, preventing occupants from performing tasks. This effect is known as disability glare. Disability glare measurably impairs vision, reducing the contrast of the retinal image by the presence of a very bright light source in the field of view (*I*). To remedy such issues after construction is expensive, and those affected must tolerate the glare until the problem is remedied. In order to address the issue of glare hazards from new constructions, this paper presents a general method for analyzing glare hazards based on three-dimensional (3D) models produced during the design phase, measured material properties and physically accurate lighting simulations.

The new method is presented through a case study analysis of glare at an airport caused by intense reflections from a PV array consisting of 2,478 panels located between the airport's air traffic control tower (ATCT) and an airplane taxiway. Specular reflections from the PV array are so extreme that they prevent the visibility of aircraft on the taxiway and cause temporary after images that impede the viewing of computer monitors inside the ATCT. As such, the reflections at the case-study airport meet the qualifications to be considered disabling.

The PV array was analyzed according to Federal Aviation Administration (FAA) best practice guidelines for the installation of solar technologies prior to its construction; however, the original analysis did not detect the glare hazard. Thus, there is a need to define a clear process through which to conduct glare prediction analysis that is useful during the design of new constructions that have the potential reflect large quantities of daylight. A case study approach is taken to address this need through an analysis of the airport's glare problem. First, a review of existing methods for analyzing glare from specular surfaces is conducted. Following that, the authors reproduce the problem in a physically-based daylighting simulation software capable of predicting reflections from new designs before they are constructed and outline steps necessary to reproduce our method. The simulations use physically accurate material models that account for specular and diffusing reflective surface properties of PV panels. Side-by-side comparisons of high dynamic range (HDR) photographs and the authors' physically-based renderings confirm the accuracy of these models. Next, an annual analysis is conducted using a ten-minute simulation interval for every daylit hour in the year. Following this, the likelihood of experiencing disability glare is displayed spatially and temporally in order to understand the time, location and intensity of potential glaring reflections. Finally, the new method is used to analyze proposed remediation strategies of the disability glare problem at the case-study airport.

QUALIFYING DISABILITY GLARE DUE TO SPECULAR REFLECTIONS

Disability glare at the case-study airport

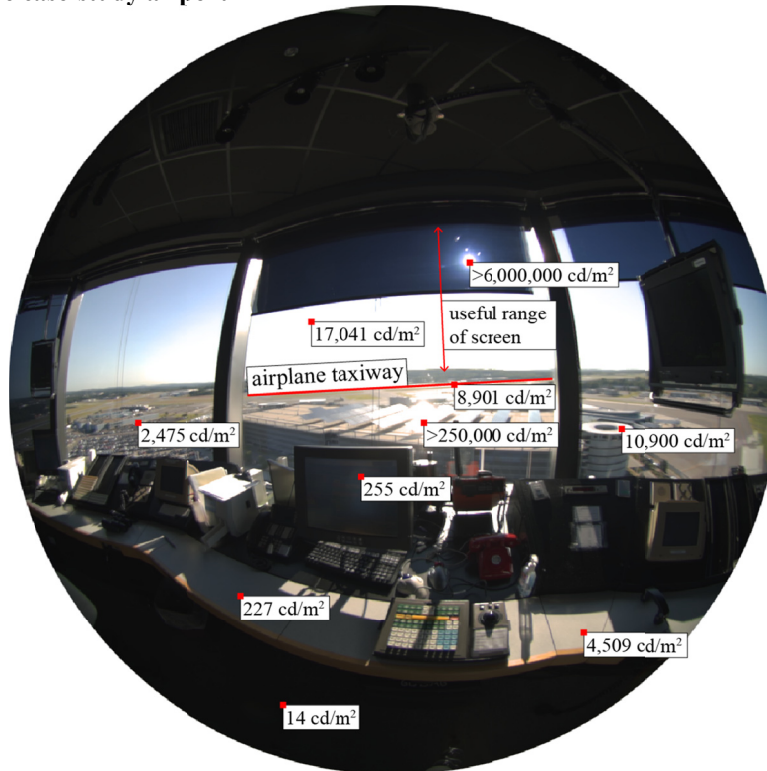


FIGURE 1 High dynamic range photograph of glare problem taken on August 30th, 2013 at 7:22 solar time.

To document the disability glare problem, the authors took HDR photographs calibrated to physical light levels from the case-study airport's ATCT. Calibrated HDR photographs record the brightness of each pixel in a photograph and can be used to calculate the likelihood of discomfort or disability glare at the time the photograph was taken. Figure 1 illustrates one such photograph with spot brightness values measured at the red squares and indicated in units of luminance (candela per square meter, cd/m^2). The method used to create such images relies upon capturing several exposures at known shutter speeds, lens apertures and exposure times. Afterwards the photos are composited and calibrated to physical values using a camera-specific calibration function based on measured luminance data with calibrated instruments. Inanici found this method to have an average error of 5.8% for outdoor scenes and 10.1% for daylight interior scenes (2). The resulting HDR photograph is stored in the Radiance RGBE image format, a lossless format where each pixel corresponds to a physical value. The authors used a Konica Minolta Ls-110 spot luminance meter to verify that values above 250,000 cd/m^2 were observed reflected from the PV panel installation.

These ultra-bright reflections cause disability glare, preventing the air traffic controllers from performing their job of seeing aircraft on the taxiway. Most indoor surfaces, with the exception of areas illuminated by direct sunlight, shown in Figure 1 have measured a luminance below 3,000 cd/m^2 . Outdoor objects are often brighter than these reference interior surfaces. At the time of observation, outdoor surface luminances were between 2,475 and 10,900 cd/m^2 . The sun, even partially obscured by the shading system, is very bright and over 6,000,000 cd/m^2 ; however, it is not directly in the field of view when looking toward the taxiway.

The very bright ($> 250,000 \text{ cd/m}^2$) reflections from the PV panels are located in the field of view when looking toward the taxiway and are much larger than the sun. The growth in size compared to that of the sun is due to an effect known as forward scattering. Forward scattering is when a direct light source is spread out in an angular opening area when reflected due to roughness and sub-surface scattering properties of the reflecting material. When an extremely bright light source such as the sun is spread across an area due to forward scattering, extreme discomfort or visual disability is likely to occur.

Dynamic Range of Human Vision

To assess the impact bright specular reflections have on perception, considering the physiology of human vision is critical. The eye is a logarithmic sensor capable of perceiving 12 log units of luminance; however, human vision is only capable of resolving a portion of the luminous scale at any given time based on the visible luminous environment (3). Specifically, the adaptation luminance is the brightness level the eye is adapted to that determines what range of the luminous scale is perceivable.

Ferwerda, et al. suggest that the adaptation luminance should be half the value of the highest perceived luminance, which will vary depending on the outside brightness, solar position, and reflectivity of glare-inducing surfaces (4); however, this works primarily for normal viewing conditions where the sun and glaring reflections are not present. In the case of disability glare analysis where the task is known, it makes sense to choose the adaptation luminance relative to the desired tasks. From Figure 1, focusing on the monitor (255 cd/m²), is the lowest task luminance level, which is reasonable considering the luminous range of a typical computer monitor is between 10 and 300 cd/m². The highest task luminance level is focusing on the taxiway (8,901 cd/m²).

Generally, the human eye can recognize between two and three orders of magnitude of luminance variation at any time (3). Taking the mean brightness of the two task luminances, approximately two orders of magnitude of luminous difference can be visualized (3, 5). This means that in order to view planes on the taxiway while maintaining the ability to read the monitor, luminance levels in the line of sight would need to be less than 30,000 cd/m² observing these two orders of magnitude as a rule. Therefore the authors propose a brightness of 30,000 cd/m² as a threshold at which the probability of experiencing disability glare is likely. The measured value of 250,000 cd/m² from the PV panels in Figure 1 is well above this threshold. Air traffic controllers attempting to view the runway experience after images and are prevented from visually identifying aircraft on the taxiway. Although the sky is very bright and often above 30,000 cd/m², the operable shades present in the ATCT can be used to block the brightness of the sky; however, they cannot be lowered to obstruct the PV array without also blocking the taxiway. Until the glare problem is remedied, the airport is covering the PV array with tarps, which prevent disability glare but have the side effect of also preventing the generation of electricity.

Existing Disability Glare Metrics from Specular Reflections

The FAA defines interference from solar panels concerning airspace penetration, reflectivity, and communication systems interference (6). As this analysis relates to visual disability, the authors are concerned with the regulations dealing with reflectivity. All solar installations at airports must include an “assessment of reflectivity including time periods when reflection may contact [the ATCT] and aircraft.” The FAA provides three methods of analyzing potential glare problems:

1. A qualitative analysis of potential impact in consultation with [air traffic control staff], pilots, and airport officials,
2. a demonstration field test with solar panels at the proposed site in coordination with FAA Tower personnel or,
3. a geometric analysis to determine days and times when an impact is predicted.

Method 1 is potentially inadequate as the involved parties may not have the experience or the ability to assess the potential glare hazards involved with the proposed PV system; however, it is probably adequate when PV panels will be installed far away from any critical visual areas. Method 2 is inadequate as the field test is performed during a single moment; however, the sun changes its position in the sky throughout the entire year. A test at a single time may miss glare hazards during other parts of the year. Method 3, geometric analysis, could analyze potential glare hazards throughout the year; however, there is currently no guidance on its implementation beyond two example figures that portray a perfectly specular reflection at four times during the year as if from a mirror. Such an analysis ignores potential glaring reflections during other times of the year. More importantly, a purely geometric analysis neglects the true behavior of reflected light from PV panels. Such an analysis could miss identifying potential glare hazards where an analysis that considers forward-scattering when daylight is reflected would not.

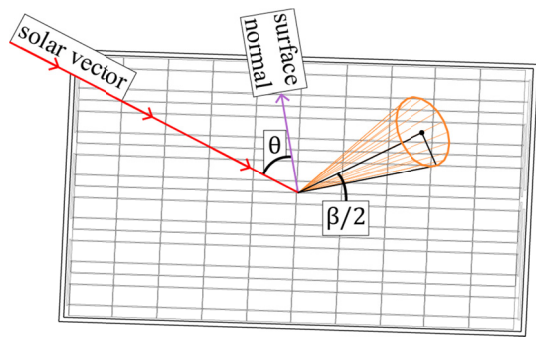
Ho et. al propose a geometric analysis method that accounts for diffuse and specular reflective properties as well as the form of a reflecting surface in order to assess glare hazards (7). The result of their geometric calculation is evaluated based on irradiance at the retina and the size of the glaring source. It is based on previous research on the physiology of the human eye to experience after images and retinal burning. The method is useful for detecting problems and quickly iterating through solutions; however, it does not provide spatial feedback regarding where the glare originates from at any given time.

METHODOLOGY

In order to analyze the current glare situation at the airport, the authors created a high-quality daylight simulation model of the ATCT, PV array, taxiway and surrounding buildings. The simulation environment used is the physically-based backward raytracer Radiance, developed at Lawrence Berkeley National Laboratory (8). Radiance is a reasonable choice as it includes a series of material modifiers that allow users to set up custom materials based on optical measurements (9) and has been validated by numerous studies (10, 11, 12, 13).

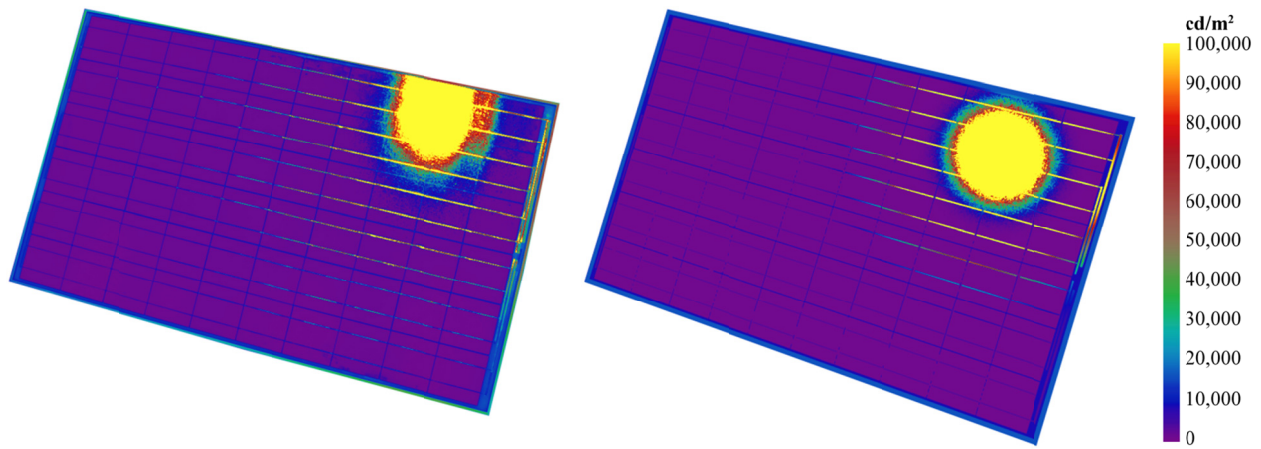
Unfortunately, detailed measured reflection data for PV panels is largely unavailable. The best practice method for resolving the complex, angular-dependent reflections from semi-specular objects such as PV panels would be to use costly goniophotometer measurements (14). Goniophotometer measurements have been used to show that measured reflections can differ from standard material models by over two orders of magnitude, especially at shallow incident angles of sunlight (15). As such measurement devices were not available for this study, the authors took measurements of the installed PV panels using a Konica Minolta 2600d portable spectrophotometer and HDR photography as documented in Table 1. The spectrophotometer measurements characterize the overall percentage of diffuse and specular reflection from the PV panel surface sampled at every 10 nm of the visible spectrum; however, the instrument is unable to resolve information about the amount of forward-scattering of specular reflections from the panel at differing incident angles of sunlight. The authors therefore quantified the forward-scattering properties based on HDR photography taken with the sun at a near-normal incidence (12 degrees) to the panel and at an oblique angle (76 degrees). This results in beam spread angles described in Table 1, which were translated into the Ashikhmin-Shirley material type in Radiance (16, 17). The Ashikhmin-Shirley material description is useful as it allows separate diffuse and specular reflection parameters, which vary significantly in the measured PV panel data. Our measurements found a total beam spread angle of between 2.0 and 9.2 degrees depending on the incident angle and area-weighted diffuse and specular reflectivities of 8.67 and 5.58 percent respectively.

TABLE 1 Measured Properties of PV Panel



Angle from normal solar incidence (θ)	Half beam spread angle ($\beta/2$)	Ashikhmin-Shirley specular exponent
12 deg.	1.0 deg.	3500
76 deg.	4.6 deg.	175
Measured area and type	Reflectance	Relative area
PV Cells Diffuse	2.56%	84.80%
PV Cells Specular	4.12%	
White Areas Diffuse	45.13%	5.62%
White Areas Specular	4.52%	
Silver Strips Diffuse	18.63%	4.47%
Silver Strips Specular	36.40%	
Frame Diffuse	61.23%	5.11%
Frame Specular	3.97%	
Area-Weighted Diffuse	8.67%	
Area-Weighted Specular	5.58%	

Figure 2 portrays an example HDR photograph of the PV panel (2a) and a rendering using the Radiance software and the author's custom materials (2b) rendered in falsecolor. In a falsecolor rendering, the color of each pixel corresponds to a physical luminance value in cd/m^2 as indicated by the colorbar scale. Such falsecolor imagery constitutes a way to assess large luminous ranges visually as they vary across a calibrated photograph or physically-based rendering. For example, yellow areas in Figure 2 reflect greater than or equal to $100,000\text{ cd/m}^2$ while dark blue areas reflect approximately $10,000\text{ cd/m}^2$. The photograph and the rendering were captured and rendered under similar clear sky conditions. Visually, the behavior of the simulation closely mimics that of the actual panel.

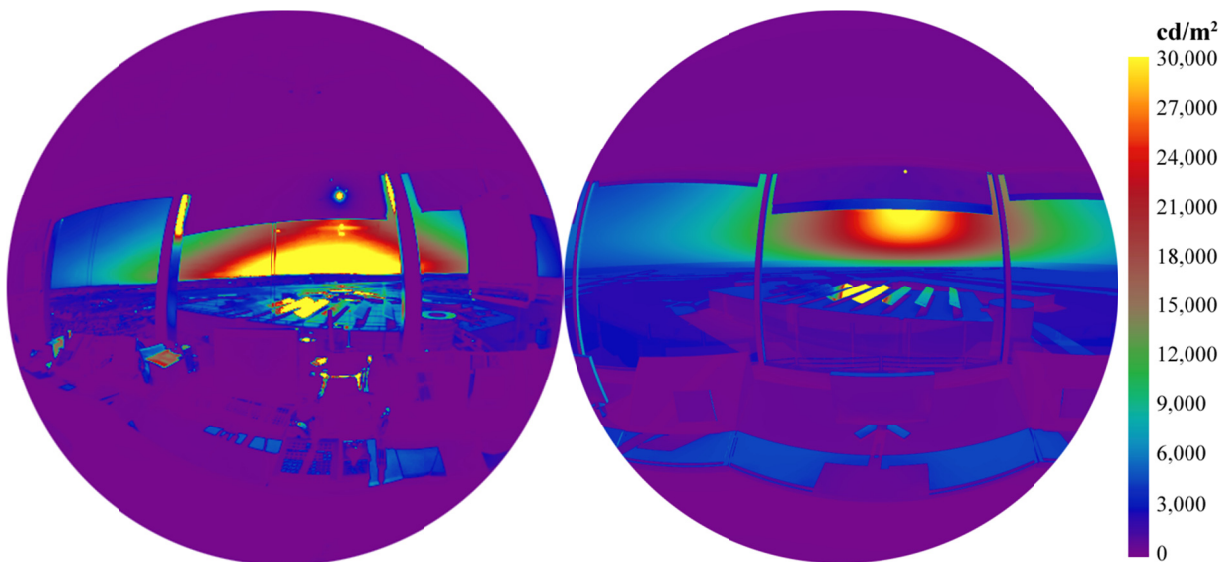


(a) High dynamic range photograph taken on August 31st, 2012.

(b) Physically-based rendering under ideal CIE clear sky conditions with sun.

FIGURE 2 Photographed and rendered falsecolor images of a single PV panel with the sun at near-normal incidence.

Apart from appropriate material descriptions, a geometrically precise 3D model is necessary to accurately reproduce the observed glaring conditions in the Radiance simulation environment. A 3D model was provided by the US Department of Transportation's Volpe center and was translated by the authors into the Radiance format. Using the 3D model and the detailed material definitions described previously, it is possible to predict the probability of disability glare for every daylight hour in the year. As a proof of concept, a HDR photograph and a Radiance rendering using the same daylight condition are compared in Figure 3. 3a is a HDR luminance photograph taken at 7:22 solar time on the morning of August 30th, 2012 from the ATCT viewing the taxiway. The image is displayed such that yellow areas correspond to brightnesses greater than 30,000 cd/m^2 . A rendering simulated at the same time is shown in 3b. Careful comparison of Figures 3a and 3b shows a very good agreement of areas greater than 30,000 cd/m^2 . Using this calibrated simulation model, it is possible to simulate the intense solar reflections from the PV panels at any time during the year in a few seconds.



(a) HDR photograph taken on 8-30-2012 at 7:22 solar time

(b) Physically-based rendering simulated for 8-30-2012 at 7:22 solar time

FIGURE 3 Imagery of glare issues seen from the ATCT.

The authors analyzed the glare potential for every ten minutes in the year assuming a CIE clear sky (18) distribution as a ‘worst case’ scenario when the sun is present and the sky is free of clouds. The analysis therefore yields the time in the year during which glare could be caused by direct sunlight being reflected from the PV panels and does not account for overcast or cloudy days. Results recording the intensity and spatial location of glaring conditions are stored in the Radiance RGBE image format, the same format as the authors’ HDR photographs.

RESULTS

In order for glare analysis to be meaningful, it is necessary to know at what time the glare occurs and where the glare originates from. To accomplish this, the analysis results are displayed temporally and spatially. This dual display is useful to assess the extent, location, and time of occurrence of disability glare from specular reflections. Figure 4 illustrates a falsecolor plot showing the perceived size of glaring reflections over $30,000 \text{ cd/m}^2$ for every ten minutes in the year. The horizontal axis contains one column for every day, the vertical axis a row for each ten minute interval, and the colors correspond to the perceived size of the glare source in solid angle steradian (str). In order to assess this chart, it is useful to note that the solid angle of an idealized viewing hemisphere is $2\pi \text{ str}$, and the solid angle of the sun viewed from Earth is roughly $6 \times 10^{-5} \text{ str}$. Annually there are 3.57 str-hrs of glaring area caused by the PV panels in the line of sight to the taxiway. This can be compared to the visibility of the sun from the ATCT of 0.18 str-hrs annually. The reflections account for a nearly 20-fold increase. The photo and rendering in Figure 3 portray a solid angle of $9 \times 10^{-3} \text{ str}$, roughly 15 times larger than that of the sun, but located in the line of sight to the taxiway.

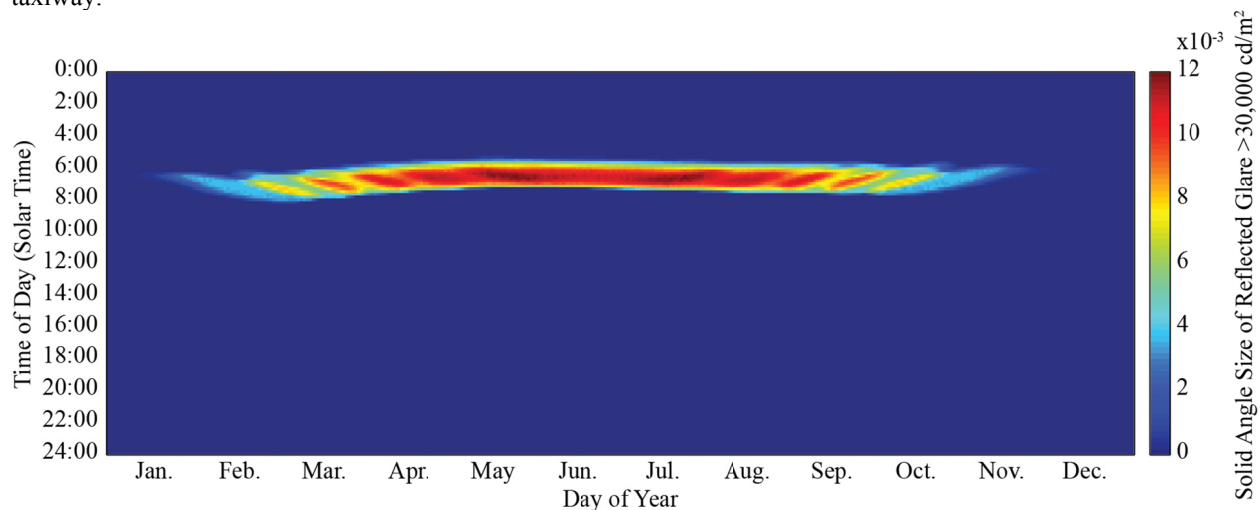


FIGURE 4 Annual temporal map showing the perceived size of reflections greater than $30,000 \text{ cd/m}^2$.

The metrics of Ho, et al. (6) can be calculated using input from rendered images such as the ones the authors create. The benefit of rendering physically-based images rather than using geometric results is that images provide spatial feedback that reveal the causes of disability glare while geometric calculations alone do not. For example in Figure 3, it is evident that disabling glare originates from the center of the PV array; however, a geometric method would only report that there is glare, not its location or intensity. To calculate Ho, et al.’s metric, the size of the glaring source in our images must be converted from a three-dimensional solid angle to a two-dimensional angle in radians. This is achieved using Equation 1 where Ω is the solid angle of the glaring reflection and ω is its equivalent in radians. The diameter of the image projected on the retina (d_r , m) can be calculated using Equation 2. Finally, the retinal irradiance (E_r) is a function of a 0.5 transmission factor, the irradiance at the cornea ($E_c, \text{W/m}^2$) and the diameter of the pupil when exposed to daylight (0.002 m) as shown in Equation 3. Using the visual conditions of Figure 3 as an example, there is a solid angle of $9.5 \times 10^{-3} \text{ str}$ brighter than $30,000 \text{ cd/m}^2$. Using Equation 1 renders an angle of $1.1 \times 10^{-1} \text{ rad}$, which equates to a $1.9 \times 10^{-3} \text{ m}$ diameter projected onto the retina. Finally, the mean irradiance at the cornea is 940 W/m^2 as derived from the authors’ simulations using Radiance’s 179 lm/W luminous efficacy. Plugging these values into Equation 3 gives a retinal irradiance of 522.8 W/m^2 . Using Ho, et al.’s metric, this irradiance and retinal projection is likely to cause after-images (6).

$$\omega = 2 \cos^{-1} \left(1 - \frac{\Omega}{2\pi} \right) \quad (1)$$

$$d_r = 0.017\omega \quad (2)$$

$$E_r = 0.5E_c \left(\frac{0.002^2}{d_r^2} \right) \quad (3)$$

Supplementing the temporal map of Figure 4, Figure 5 shows in falsecolor the location of glaring reflections throughout the year in hours above 30,000 cd/m² with the scale ranging between 0 and 60 hours. Purple-colored areas cause no glare, and yellow-colored areas cause 60 or greater hours of glare annually. As each rendered photograph in the Radiance RGBE image format has a physical luminance value associated with each pixel, by adding 1 for every timestep when a pixel is over 30,000 cd/m² and then dividing by 6 – the number of ten minute intervals within an hour – spatial representations of the glare problem are quickly and easily created. In the figure, labels for each row in the PV array are applied from A1 to C3. The bottom corner of row C2 and all of row C3 do not cause glare; therefore, it is likely that if the PV array was located further north, no glare problems would occur. Such an image would have provided valuable feedback during the design of the PV array.

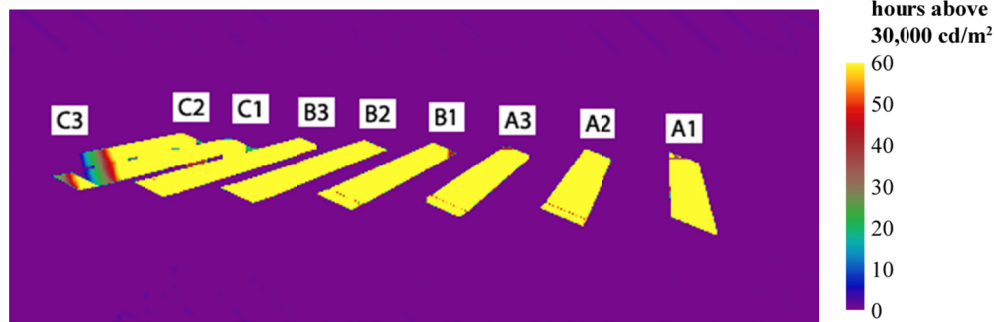


FIGURE 5 Annual hours of predicted glare under CIE clear sky conditions with sun.

As discussed earlier, the airport is covering parts of the PV array that cause glare with tarps in order to prevent disability glare from occurring. The author’s method was used to plan when each row should be covered throughout the year until remediation methods can be taken. Figure 6 illustrates monthly falsecolor hours of occurrence of glaring reflections for half of the year from July 1st to December 31st generated using an identical methodology to that of Figure 5 but using monthly intervals. For example, in July rows B2 – C2 should be covered with tarps; however, in November it is only necessary to cover row A1. In December all rows can be left uncovered in order to maximize PV electric production as there is no likelihood of glare from specular reflections. Figure 6 also clearly portrays that doing a spot field test of PV panels as possible in the FAA’s guidelines can be insufficient. For example, if a field test was done in July, no glare would be detected for panel rows A1-B1; however, those rows cause glaring reflections in September, October and November.

DISCUSSION

In the results section, it is shown that the new image-based analysis method can identify glare problems during the design of a PV system based on sky models that accurately resolve the solar position, appropriate material representations and a complete 3D model. Furthermore, the occurrence of glare can be displayed temporally and spatially. It is therefore useful to employ the method to detect potential new glare hazards in proposed remediation strategies. The authors evaluated two remediation options developed in concert with the airport staff. Option 1 was to replace the PV panel with a less-reflective panel. Option 2 was to rotate the entire array 90 degrees such that it faces away from the ATCT. These two options constitute typical material and formal changes that may occur during a PV array design process. Other options, including constructing exterior shading systems on the ATCT or the parking structure, were not considered due to regulatory pressures and their potential size (five stories tall in the case of a vertical shading device on the parking structure).

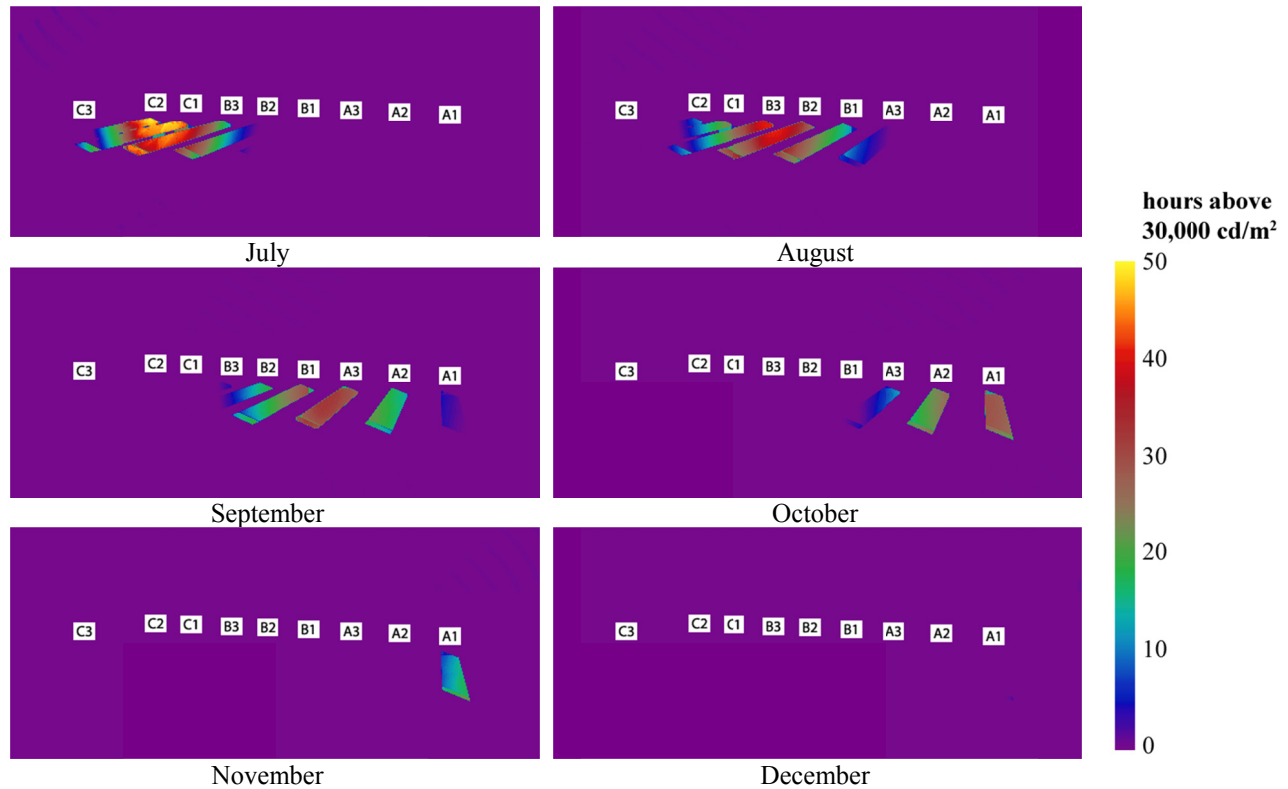


FIGURE 6 Selected monthly images showing hours of predicted glare under CIE clear sky conditions with sun.

Option 1: A Less Reflective PV Panel

A potential replacement panel was measured using the same process as documented in Table 1, which resulted in an area-weighted diffuse reflectance value of 4.73% and an area-weighted specular reflectance value of 2.97%, which means the proposed panel reflects 45.3 and 46.8 percent less light respectively than the installed panel. The new simulation and analysis process was used to investigate whether this substantial reflective reduction is enough to solve the glare problem. Before describing the results, it is worthwhile to consider the case of the photograph in Figure 1, where the PV panels had a measured brightness of over 250,000 cd/m². Half of this value is 125,000 cd/m², a substantial reduction; however, it is still much higher than our defined comfort threshold of 30,000 cd/m². Therefore, in the case of Figure 1, a less-reflective panel will not correct the glaring situation unless the panel is substantially less forward-scattering.

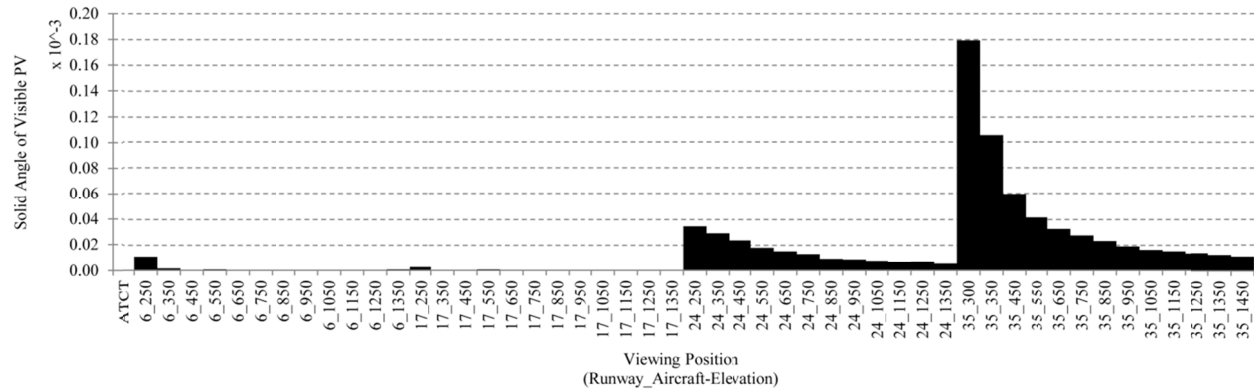
The less reflective PV panels do cause a perceptible glare decrease. The reflections would always be less bright as noted above; however, the annual glaring area decreases only 8.0% to 3.29 str-hrs. This meager decrease is because during clear sky conditions even the reduced specular reflections of the improved panel are bright enough to cause disability glare.

Option 2: Rotate the Panels 90-degrees to the East, Away from the ATCT

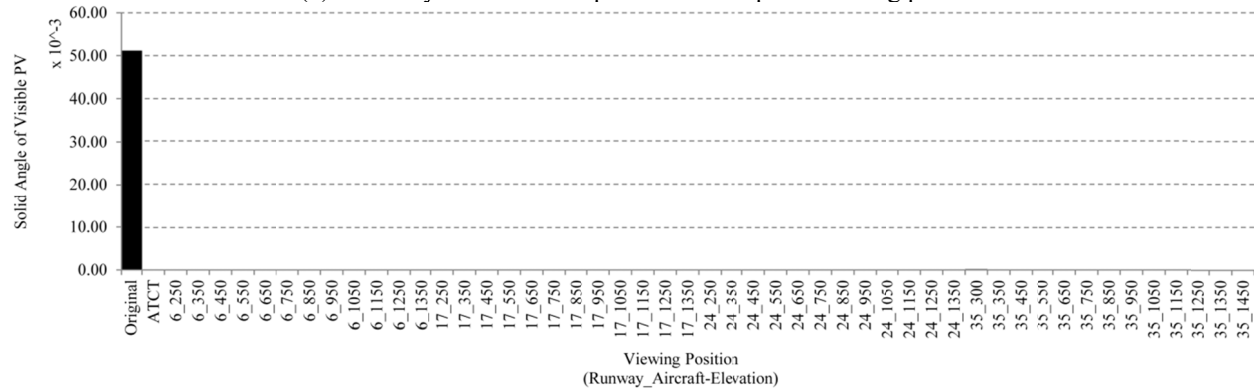
A geometric solution to rotate the panels such that they face away from the ATCT was explored. By rotating the panels 90 degrees counter-clockwise, they will face southeast and away from air traffic operators. In this way, the operators can no longer see the reflective face of the PV panels. This was confirmed using annual simulations using an identical process to those shown in Figure 4. One concern was that by rotating the PV panels to face away from the ATCT, a new glare hazard may be created for pilots.

Before assessing disability glare potential for each position along the landing paths, it is worthwhile to investigate the potential for glare. It is possible to determine the visible size of the PV panels which is exactly the maximum potential for the size of a reflected glare source. The case-study airport has four landing paths which were analyzed at every 100 vertical feet of descent. The maximum visibility of the solar panels is from runway 35 at 300 feet above sea level (just before landing) with a visible solid angle of 1.8×10^{-4} sr or 0.0029% of the visual hemisphere. For reference this is 2% of the glare size observed on August 30th 2012, depicted in Figure 3. The visible solid angle sizes of the proposed redesign of the PV array are shown in Figure 7a from the ATCT and along

the various landing paths. To reinforce what this 2% means, Figure 7b adds an extra data point, the current visibility of the PV array from the ATCT (5×10^{-2} sr). When comparing PV visibility, the maximum possible glaring reflection, from the aircraft landing paths to the existing visibility of PVs from the ATCT, there is very little potential for pilots to experience glare. Further, the potential for air traffic controllers to experience glare is now zero as they only see only the back sides of the PV panels.



(a) Visibility of rotated PV panels from airplane landing paths.



(b) Visibility of rotated PV panels from airplane landing paths compared against the original visibility of PV panels from the ATCT.

FIGURE 7 Solid angle of visible area of PV in steradian from the ATCT and landing paths.

CONCLUSIONS

This case study illustrates the potential for physically-based renderings to analyze proposed new constructions that use specular materials in critical situations such as at airports. The new method of analysis is appropriate for the specular surfaces of PV panels; however, it is also appropriate for other constructions such as buildings with a large amount of glazing or bodies of water. The authors have shown that simulations closely mimic the behavior of physical reflections when using appropriately calibrated material models. A new maximum visible luminance value of $30,000 \text{ cd/m}^2$ in the line of sight has been proposed based on the physical ability of the eye to resolve items beyond that threshold when also viewing a typical computer screen. This upper luminance limit was applied to the analysis of an airport with a known disability glare problem.

An issue identified in this study is that the analysis guidelines proposed in the FAA's "Technical Guidance for Evaluating Selected Solar Technologies on Airports" document are vague and allow analysis that does not account for the physical reality of reflections from PV panels or that does not account for differing solar positions throughout the year. Had the analysis method proposed in this study or that of Ho, et al. been utilized, the glare problem likely would have been identified before construction.

A significant barrier to such analysis is that measured material data from PV panels is largely not available in practice. This makes it nearly impossible to compare the benefits of choosing between different PV panels or specular materials. In order for meaningful analysis to be made in the future, detailed angular-dependent material measurements (14) need to be performed and made available for a wide variety of potential construction materials that may be used in critical situations.

After using a HDR photographic method to derive angular-dependent material reflection data, the authors undertook an annual analysis of the case-study airport with a known occurrence of disability glare. The new method produces charts (Figure 4) that illustrate the time and intensity of glaring reflections and images (Figures 5 and 6) that show the location of glaring reflections. Such results allow intuitive design changes based on observations. For example, Figure 5 suggests that a more northern site for the PV array would have been beneficial. The authors' new method was used to analyze two proposed remediation strategies. This analysis found that a material solution using a less-reflective PV panel was not viable in this case, but that a geometric solution to rotate the PV panels would remedy the glare hazard.

REFERENCES

1. Commission Internationale de l'Eclairage. *Discomfort Glare in Interior Lighting*. CIE Publication 117, 1995.
2. Inanici, M. N. *Evaluation of High Dynamic Range Photography as a Luminance Data Acquisition System*. *Lighting Research and Technology*, Vol. 38, No. 2, 2006, pp. 123-34.
3. Boyce, P. R. *Human Factors in Lighting, Second Edition*. Taylor & Francis Inc., New York, 2003.
4. Ferwerda, J. A., S. N. Pattanaik, P. Shirley, and D. Greenberg. *A Model of Visual Adaptation for Realistic Image Synthesis*. Proceedings of ACM SIGGRAPH '96, pp. 249-58.
5. Hopkinson, R. G. and J. B. Collings. *The Ergonomics of Lighting*. Macdonald & Co., 1970.
6. Federal Aviation Administration, Office of Airports, Office of Airport Planning and Programming, Airport Planning and Environmental Division (APP-400). *Technical Guidance for Evaluating Selected Solar Technologies on Airports*. http://www.faa.gov/airports/environmental/policy_guidance/media/airport_solar_guide.pdf. Accessed May 9, 2013.
7. Ho, C. K., C. M. Ghanbari and R. B. Diver. *Methodology to Assess Potential Glint and Glare Hazards from Concentrating Solar Power Plants: Analytical Models and Experimental Validation*. *Journal of Solar Energy Engineering*, Vol. 133, No. 3, 2011.
8. Ward, G. J. *The RADIANCE Lighting Simulation and Rendering System*. Proceedings of the 21st Annual Conference on Computer Graphics and Interactive Techniques, 1994, pp. 459-72.
9. Reinhart, C. F. and M. Andersen. *Development and Validation of a Radiance Model for a Translucent Panel*. *Energy and Buildings*, Vol. 38, No. 7, 2006, pp. 890-904.
10. Mardaljevic, J. *Validation of a Lighting Simulation Program Under Real Sky Conditions*. *Lighting Research and Technology*, Vol. 27, No. 4, 1995, pp. 181-8.
11. Reinhart, C. F. and O. Walkenhorst. *Validation of Dynamic RADIANCE-based Daylight Simulations for a Test Office with External Blinds*. *Energy and Buildings*, Vol. 33, No. 7, 2001, pp. 683-97.
12. Reinhart, C. F. and P. F. Breton. *Experimental Validation of Autodesk® 3ds Max® Design 2009 and Daysim 3.0*. *Leukos*, Vol. 6, No. 1, 2009.
13. Ibarra, D. and Reinhart, C. F. *Solar Availability: A Comparison Study of Irradiation Distribution Methods*. Proceedings of Building Simulation 2011: 12th Conference of International Building Performance Simulation Association, 2011, pp. 2627-34.
14. Apian-Bennewitz, P. and J. von der Hardt. *Enhancing and Calibrating a Goniophotometer*. *Solar Energy Materials and Solar Cells*, Vol. 54, No. 1, 1998, pp. 309-22.
15. PAB Advanced Technologies, Ltd. *BME BSDF Data*. http://www.pab.eu/gonio-photometer/demodata/bme/ward_metal_ps.anofol606.37.385/index.html. Accessed July 1, 2013.
16. Ashikhmin, M. and P. Shirley. *An Anisotropic Phong BRDF Model*. *Journal of Graphics Tools*, Vol. 5, No. 2, 2000, pp. 25-32.
17. Ward, G. *What's New in Radiance for 2013*. <http://www.radiance-online.org/community/workshops/2012-copenhagen/Day2/Ward/RadianceImprovements.pdf>. Accessed January 15, 2013.
18. Commission Internationale de l'Eclairage. *Spatial Distribution of Daylight - CIE Standard Overcast Sky and Clear Sky*. CIE Publication S003, 1996.